"Welding sequence analysis in three dimensional weldments with experimental verification"

Hernández Arriaga Isaac[a,b], Aguilera Gómez Eduardo[c], Pérez Meneses Joaquín[a]

[a]*Instituto Tecnológico de Querétaro, Av. Tecnológico S/N Esquina Gral. M. Escobedo, 76000, Querétaro,Qro., México.*
[b]*CIATEQ A.C. Centro de Tecnología Avanzada, Av. del Retablo 150, Col. Constituyentes Fovissste, 76150, Querétaro, Qro., México.*
[c]*Universidad de Guanajuato, Campus Irapuato-Salamanca, Carretera Salamanca-Valle de Santiago, 36885, Salamanca, Gto., México.*
*****Autor contacto.Dirección de correo electrónico: isaac.hernandez@ciateq.mx*

RESUMEN

En este trabajo se estudia los efectos de las secuencia de soldadura en los esfuerzos residuales y distorsión en una estructura simétrica tridimensional. Las secuencias de soldaduras apropiadas están basadas en la hipótesis de que las secuencias de soldaduras utilizadas en estructuras bidimensionales pueden ser aplicadas a estructuras tridimensionales. La metodología aplicada a estructuras bidimensionales para reducir esfuerzos residuales, distorsión o una relación entre ambos parámetros fue desarrollado en trabajos previos por el autor principal. Para realizar el análisis de la secuencia de soldadura se utilizó la técnica de elementos finitos mediante un modelo termo-mecánico secuencialmente acoplado. Los resultados de las simulaciones numéricas de la estructura tridimensional son comparados con pruebas experimentales. Finalmente, esta investigación presenta un procedimiento para determinar las secuencias de soldadura apropiadas para reducir los esfuerzos residuales la distorsión o una relación entre ambos parámetros para estructuras tridimensionales simétricas.

ABSTRACT

In this investigation, a study of the effects of the welding sequence on residual stresses and distortion in a 3-dimensional symmetrical structure is developed. Selected welding sequences reduce residual stresses, distortion, or the relation between both parameters. These proper welding sequences are based on the hypotheses of that the welding sequence to reduce residual stress, distortion, or relation between both parameters in 2-D symmetrical structures can be applied to 3-D symmetrical structures. The 2D structures methodology to reduce residual stress, distortion or a relation between both parameters was developed in previous works by principal author. To perform the numerical welding sequences analysis, a sequentially-coupled thermo-mechanical model by finite element method is developed. The results of the numerical simulations of the 3-D symmetrical structure are compared with experimental tests. Finally, this investigation presents a procedure to determine the proper welding sequences to reduce residual stress, distortion or the relation between both parameters for 3-dimensional symmetrical structures.

Keywords: Welding sequence, Residual stress, distortion.

1. Introduction

During the heating and cooling cycle in the welding process, thermal strain occurs in the filler material and in the base metal regions close to the weld. The strain produced during heating is accompanied by plastic deformation. The non-uniform plastic deformation that occurs in the welded structure is what leads to residual stresses. These residual stresses react to produce internal forces which must be equilibrated and cause distortion [1].

The residual stress and distortion in weldments depend on several interrelated factors such as thermal cycle, material properties, structural restraints, welding conditions and geometry [2]. Of these parameters, the thermal cycle has the greatest influence on the thermal loads in the welded structures. At the same time, the temperature distribution is a function of parameters such as welding sequence, welding speed, energy of the source, and environmental conditions.

A high level of tensile residual stresses near of the weld bead can induce brittle fracture, cracking due to corrosion stress, and reduced fatigue strength. Compressive residual stresses in the base metal located some distance away from the weld line can substantially decrease the critical buckling stress [3]. The main effects of distortion are the loss of tolerance in the welded components and deformation of structural elements that results in inadequate support to transfer applied loads [4]. Therefore, residual stresses and distortion should be reduced to meet all geometry and strength requirements.

Some of the most popular methods for reducing residual stresses and distortion in weld fabrication are: welding sequence [5-14], definition of welding parameters [15-17], definition of weld procedure [18], use of precambering, fixtures and prebending [19-22], thermal tensioning [23-25], heat sink welding [26], preheating [27,28], post-weld treatment [29-31], and post-weld corrective methods [32-35].

The control methods previously mentioned can increase the production costs due to energy consumption, time, and/or expensive equipment. Other methods slow down production by requiring fixture devices. Welding sequence

is inexpensive because it directly affects the temperature field of the welded structure, and consequently the residual stresses and distortion. Therefore, sequence analysis is fundamental for controlling residual stresses and distortion in welded structures.

1.1. Welding sequence background

Teng and Peng [5] investigated the reduction in residual stresses caused by welding by analyzing the effects of welding sequence on residual stress distribution in single and multi-pass butt-welded plates and circular patch welds. The research was conducted through finite element-based thermo elastic plastic analysis and simulated weld thermal cycles. Ji and Fang [6] investigated the influence of welding sequence on the residual stresses of a thick plate. Authors worked with double V-groove multiple-pass butt-welds and adopted the converse welding method between adjacent layers, or between adjacent weld beads in every layer (the converse welding method consists of applying the opposite direction between adjacent layers in multi-layer weld, or between beads in every layer). They analyzed a coupled thermo-mechanical model using finite element and an ellipsoidal heat source. The numerical results were validated against experimental results (the x-ray method). Nami, Kadivar and Jafarpur [7] investigated the effects of the welding sequence on the thermal and mechanical response of the thick plate weldments using a 3-D thermo-viscoplastic model. Anand´s viscoplastic model was used to simulate the rate dependent plastic deformation of welded materials. Also, they considered the temperature dependence of thermal and mechanical properties of material, welding speed, welding lag, and the effect of the filling material added to the weld. The model was compared with the results of two analytical and experimental works.

Mochizuki and Hayashi [8] investigated the residual stress in large-diameter, multi-pass, butt-welded pipe joints for various welding sequences. The pipe joints had an X-shaped groove. The mechanism that produces residual stress in the welded pipe joints was studied in detail using a simple prediction model. The authors worked with a thermo-elastic-plastic analysis using finite element method with an axisymmetric model. Also, they determined an optimum welding sequence for preventing stress-corrosion cracking from the residual stress distribution. Mochizuki, Hattori and Nakakado [9] studied the effect of residual stress on fatigue strength at a weld toe in a multi-pass fillet weld joint. The residual stress in the specimen was varied by controlling the welding sequence. They calculated the residual stresses by thermo-elastic-plastic analysis and compared them to strain gage and X-ray diffraction measurements. Tsai and Park [10] studied the distortion mechanisms and the effect of the welding sequence on panel distortion. In this study, distortion behaviors, including local plate bending and buckling, as well as global girder bending, were investigated using finite element analysis. It was found that buckling does not occur in structures with a skin-plate thickness of more than 1.6 mm, unless the stiffening girder bends excessively. They applied the joint rigidity method (JRM) to determine the optimum welding sequence for minimum panel warping. The JRM consists of starting with more rigid joints and progressively moving toward less rigid joints [10].

Hackmair and Werner [11] investigated the welding sequence and its effect on distortion in a T-joint structure. The T-joint structure is formed by two hollow extrusions of a 6060 T6 aluminum alloy. The extrusions are joined by four weld operations, whose order of application defines the two different welding sequences. Bart, Deepak and Kyoung [12] investigated the effect of the welding sequence on a sub-assembly composed of thin-walled aluminum alloy extruded beams. The main factor considered was the quality of the assembly after welding, which was measured by the deformation at pre-defined critical locations. The aluminum alloy extruded beam structure was modeled with a 2-D beam element model. Their methodology consisted of applying pre-estimated angular shrinkages for each welding step, thus eliminating the use of a complex nonlinear transient analysis, which would require consideration of thermo-mechanical interactions and plasticity. Two distortion modes (angular shrinkage and tilting shrinkage) were investigated and applied to welding distortion model.

Kadivar, Jafarpur and Baradaran [13] utilized a genetic algorithm method with a thermo-mechanical model to determine an optimum welding sequence. The thermo-mechanical model developed for this purpose predicts the residual stress and distortion in thin plates. The thermal history of the plate was computed with a transient, two dimensional finite element model which serves as an input to the mechanical analysis. The mechanical response of the plate was estimated through a thermo-elastic, viscoplastic finite element model. The proposed model was verified by comparison with available experimental data. The authors observed that the welding sequence changes the distribution of residual stress, but has little influence on the maximum residual stress levels. However, the welding sequence does have an effect on the weldment distortion. Therefore, the authors chose the minimization of distortion as the target function. Voutchkov, Keane, Bhaskar and Olsen [14] proposed a surrogate model that substantially reduces the computational expense in sequential combinatorial finite element problems. The model was applied to a weld path planning problem in a tail bearing housing (TBH). The TBH is a crucial component of most gas turbines and is used to help mount the engine to the body of the aircraft. The welding sequence used to attach the vanes to the inner ring was chosen to minimize distortion during the welding process.

2. Finite element model

The proposed sequentially-coupled thermo-mechanical analysis involves two steps: a transient heat transfer analysis is performed followed by a thermal elastic plastic analysis.

2.1. Thermal model

The governing equation of the heat flow follows the first law

of thermodynamics (conservation of energy). This law states that the rate of change of internal energy ρcdT and conduction $\nabla \cdot q$ must be in equilibrium with the heat production Q and the power of elastic and viscoplastic straining ε^e and d^{vp}, respectively [36]:

$$\rho c \frac{\partial T}{\partial t} + \nabla \cdot q = Q - \frac{E \alpha T}{1-2\nu} \dot{\varepsilon}^e + \xi s d^{vp} \quad (1)$$

The parameter ξ takes on the value of 1 if all inelastic dissipation sd^{vp} is converted into heat. The mechanical coupling terms in (1) are in most cases not considered because their influence on the temperature field is very small [37]. It is therefore possible to divide the thermo-mechanical analysis of a welding process into two main parts: the analysis of the temperature field and subsequent analysis of the mechanical fields.

Neglecting the mechanical coupling terms in Eq. (1), the energy equation becomes [37]:

$$\rho C \frac{\partial T}{\partial t} + \nabla \cdot q = Q \quad (2)$$

Equations (1) and (2) are statements of the First Law of Thermodynamics [38]. Fourier's law of heat transfer defines a relationship between the heat flux q and the gradient of the temperature field ∇T . For an isotropic material this relationship is the Fourier heat conduction law:

$$q = -k \nabla T \quad (3)$$

Where k is the thermal conductivity for the material. Equation (2) and (3) give

$$\rho C \frac{\partial T}{\partial t} = \nabla \cdot (k \nabla T) + Q = (\{L\}^T [D] \{L\} T) + Q \quad (4)$$

In Cartesian coordinates x, y, z, equation (4) becomes

$$\left[\frac{\partial}{\partial x}\left(k_x \frac{\partial T}{\partial x}\right) + \frac{\partial}{\partial y}\left(k_y \frac{\partial T}{\partial y}\right) + \frac{\partial}{\partial z}\left(k_z \frac{\partial T}{\partial z}\right)\right] + Q(x, y, z, t) = \rho C \frac{\partial T(x,y,z,t)}{\partial t} \quad (5)$$

Where k_x, k_y, k_z is the thermal conductivity in the x, y and z directions, respectively, $T(x, y, z, t)$ is the temperature, ρ is the density, C is the specific heat and t is time. Equation (5) becomes nonlinear if material properties k_x, k_y, k_z, ρ, and C are a function of temperature. The first term is conduction of heat through the material. The second term $Q(x, y, z, t)$ is the source of heat generation. The last term is the rate of change of internal energy.

2.2. Mechanical model

In the mechanical analysis, the temperature history obtained from the thermal analysis is introduced as a thermal loading. Thermal strains and stresses can be calculated at each time increment, and the final state of residual stresses will be accumulated by thermal strains and stresses. Residual stresses in each temperature increment are added to those at nodal points to update the behavior of the model before the next temperature increment.

Three basic sets of equation relating to the mechanical model, the equilibrium and compatibility equations and the constitutive equations for thermal elastic plastic material, are considered as follows [1]:

$$\sigma_{ij,j} + f_i = 0 \quad (6)$$

Where f_i is the sum of the body force and σ_{ij} is the Cauchy stress tensor. To ensure that the body remains continuous during the deformation, the compatibility equations must be satisfied [2]:

$$\varepsilon_{ij,kl} + \varepsilon_{kl,ij} - \varepsilon_{ik,jl} - \varepsilon_{jl,ik} = 0 \quad (7)$$

The thermal elastic plastic material model will be derived assuming isotropic material, Von Misses yield criterion and the associated flow rule and linear isotropic hardening. Thermal and mechanical properties of the selected material are a function of temperature. The micro-structural evolution is not considered. The initial assumption is that the total strain increment can be decomposed as (valid for small strains and rotations) [1]:

$$d\varepsilon_{ij} = d\varepsilon_{ij}^e + d\varepsilon_{ij}^p + d\varepsilon_{ij}^\theta \quad (8)$$

The thermo-mechanical analysis involves two steps. First, a transient heat transfer analysis is performed. The calculated transient temperatures are applied as a step-by-step thermal load. In the second step, a thermal elastic plastic analysis (quasi-static) computes the cumulative thermal stresses for each time step. The end result is residual stress and distortion.

PLANE55 and SOLID70 elements are selected for two and three dimensional thermal analysis, respectively. Both elements have a single degree of freedom, temperature and isotropic material properties [39]. PLANE42 and SOLID45 elements are selected for two and three dimensional structural analysis, respectively. PLANE 42 and SOLID45 elements have two and three degrees of freedom at each node, respectively: translation in the nodal directions and isotropic material properties [39].

Temperatures vary widely within the welded part. Therefore, thermal and mechanical properties of welded materials vary significantly [40]. The thermal and mechanical properties of ASTM A36 due to temperature are shown in Fig. 1. Autogeneous weldment was assumed. These means that weld metal, heat affected zone (HAZ), and base metal share the same thermal and mechanical properties [40].

The heat loading is simulated via weld thermal cycle curves shown in Fig. 2. The input heat is applied to all surfaces between the weld metal and the base metal.

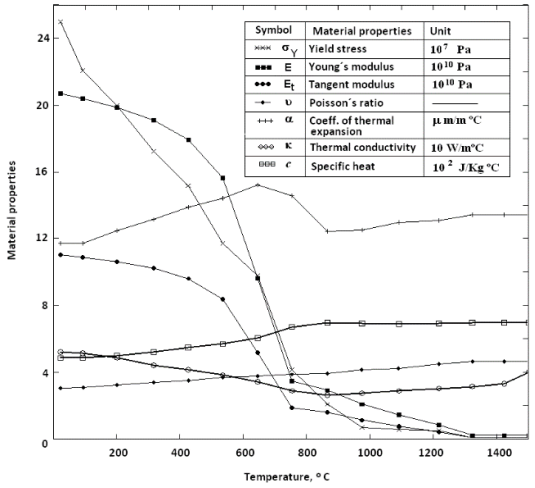

Figure 1. Thermal and mechanical properties of ASTM A36 as a function of temperature [40].

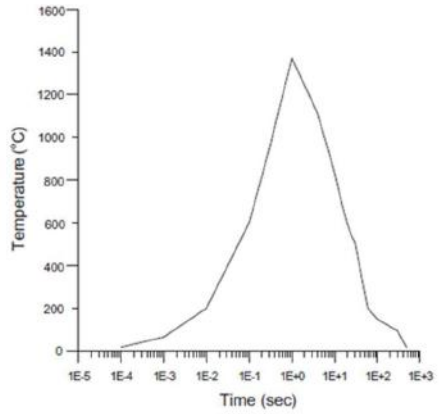

Figure 2. Weld thermal cycle of ASTM A36 carbon steel [40].

3. Welding sequence analysis in a 3-d symmetrical structure

This study describes the effects of the welding sequence on the residual stresses and distortion in a 3-D unitary cell, with the purpose of demonstrating that the methodology developed in previous work [41] for determining the proper welding sequences to reduce residual stress, distortion, or the relation between both parameters in 2-D symmetrical structures can be applied to 3-D symmetrical structures, where weld bead circles now become spheres.

3.1. Hypothesis to determine the proper welding sequence to reduce the residual stress, distortion, or a relation between both parameters in 3-D symmetrical structures

To determine the proper welding sequences to reduce the residual stress, distortion, or a relation between both parameters in 3-D symmetrical structures, we start by identifying the axis of symmetry and the center of gravity of the structure. Next, we draw concentric spheres centered on the center of gravity of the structure, and extending to the center of gravity of each of the weld beads. Weld beads located at the same distance from the center of gravity of the structure will fall on the same sphere. The spheres are numbered from the smallest to the largest.

a) To reduce residual stress: Start with the weld beads belonging to the smallest sphere and then continue with the weld beads belonging to the larger adjacent sphere until the largest sphere is reached. The weld beads belonging to the same sphere should be symmetrical. First, the beads with diagonal symmetry are selected. If the weld bead with diagonal symmetry has already been selected, then the farthest symmetrical weld bead is selected next. When a current weld bead has more than one farthest symmetrical bead, the adjacent weld bead in counter-clockwise is selected. Finally, to move from one sphere to the other, the farthest weld bead to the current bead is selected. If a current bead has more than one farthest weld bead, the adjacent bead in counter-clockwise is selected. The converse welding method between weld beads is adopted.

b) To reduce distortion: Apply welding tacks to the structure before welding. First, the weld beads in the largest sphere are selected and then the weld beads belonging to the adjacent smaller sphere are selected until the smallest sphere is reached. The application of the weld beads on the same sphere should be in symmetrical form. The weld beads with diagonal symmetry are selected first. If the weld bead with diagonal symmetry has already been selected, then the farthest symmetrical bead is selected next. When a weld bead has more than one farthest symmetrical bead, the adjacent weld bead in counter-clockwise direction is selected next. Finally, to move from one sphere to the other, the farthest weld bead to the current is selected. If a weld bead has more than one farthest bead, the adjacent bead in a clockwise direction is selected. The converse welding method between beads is adopted.

c) To improve the relation between residual stress and distortion: Start with the weld beads on the smallest sphere and then continue with the weld beads on the larger adjacent sphere until the largest sphere is reached. The application of weld beads on the same sphere should be in an adjacent form in counter-clockwise direction. To move from one sphere to the other, the closest weld bead to the current bead is selected. The converse welding method between weld beads is adopted.

3.2. Geometric configuration of the 3-D unitary cell

A 3-D unitary cell configuration is selected because it is a common structural arrangement in industry, used in the construction of panels, ships, bridges, etc. This configuration keeps the requirement of symmetry in the space. The 3-D unitary cell consists of two horizontal and

two vertical plates joined by fillet welds as shown in Fig. 3.

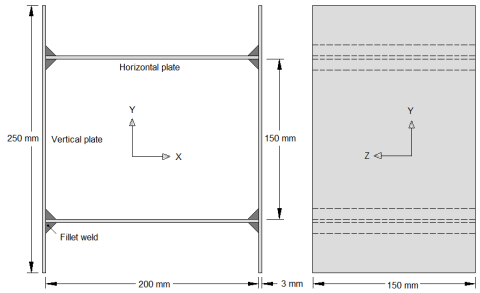

The thickness of the plates is 3 mm.

Figure 3. Configurations and dimensions of the 3-D unitary cell.

3.3. Selection of the number of weld beads in the 3-D unitary cell

The 3-D unitary cell is joined by eight fillet welds. The effect of dividing a fillet weld into sub-welds is studied. For the present investigation, each of the fillet welds is divided in 3 sub-welds.

3.4. Symmetry axis selection and formation of the concentric spheres in the 3-D unitary cell

Due to the multiple symmetry (symmetry and diagonal symmetry axis) of the 3-D unitary cell, the center of mass coincides with the centroid of the structure, which is also the center of the spheres. Two concentric spheres are formed with 8 weld beads and four concentric spheres with 24 weld beads (Fig. 4).

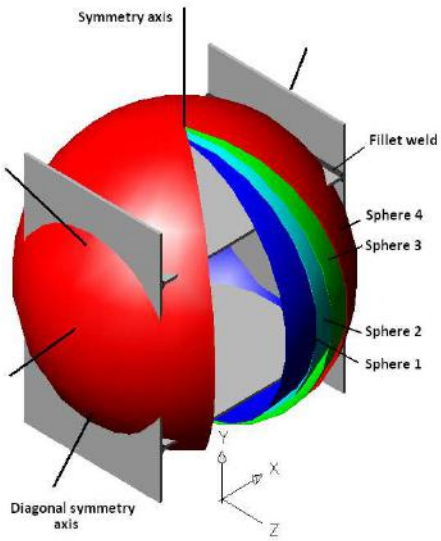

Figure 4. Axis of symmetry and concentric spheres of the 3-D unitary cell formed by 24 fillet welds.

3.5. Proper welding sequence to reduce the residual stress and proper welding sequence to reduce the distortion in the 3-D unitary cell

Figs. 5 (a) and (c) depict the proper welding sequence to reduce distortion with 8 and 24 fillet welds, respectively. Figs. 5 (b) and (d) depict the proper welding sequence to reduce the residual stresses with 8 and 24 fillet welds, respectively. These welding sequences are determined from the hypothesis made in section previous.

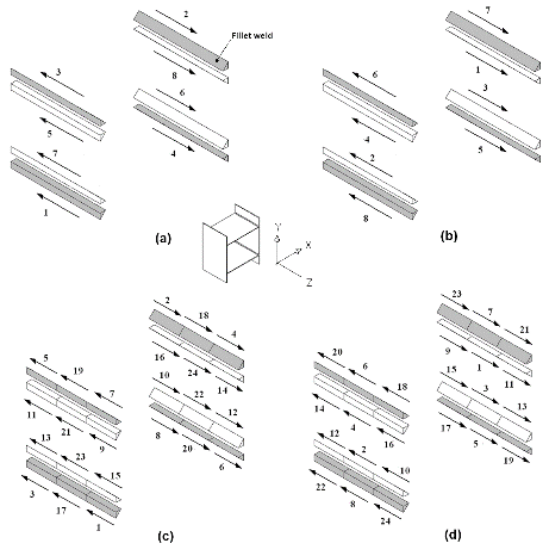

Figure 5. Different welding sequences for the 3-D unitary cell.

3.6. Material selection of the 3-D unitary cell

S235JR structural steel is selected to define the material properties of the 3-D unitary cell. This steel is widely used in Europe (Poland: steel ST3S) for construction of ships, buildings, bridges and machinery. This steel is easy to weld because of its carbon content (0.22% C) and chemical composition. The mechanical and thermal properties of the S235JR steel are similar to ASTM A36 structural steel. Steel S235JR is therefore modeled using properties of ASTM A36 structural steel.

3.7. Finite element model of the 3-D unitary cell

The numerical simulations of the welding sequences for the 3-D unitary cell are based on the numerical model of welding process developed previously. The numerical model of the 3-D unitary cell is divided into 29,362 hexahedral elements and 41,202 nodes. Fig. 6 shows the finite element model of the 3-D unitary cell.

Thermal initial and boundary conditions

(a) Initial condition: Because the thermal model consists of

a transient heat transfer analysis, it is required an initial condition of the base metal, which is considered as the surrounding temperature (T_0=20°C).

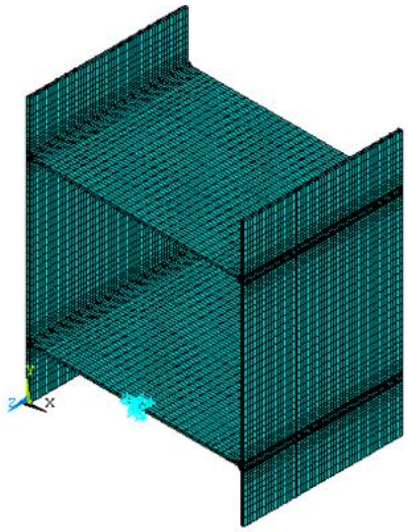

Figure 6. Finite element model of the 3-D unitary cell.

(b) Boundary conditions (see Fig. 6):

1) Surfaces in contact with the surrounding except surfaces belonging to the weld beads.

$$\kappa\frac{\partial T}{\partial n}(x,y,z,t) = -h_c[T_\infty - T_s] \quad (9)$$

2) Nodes belonging to weld beads (according to the welding sequence).

$$\kappa\frac{\partial T}{\partial n}(x,y,z,t) = q_s \quad (10)$$

Prescribed heat input: heat loading is simulated via weld thermal cycle curves (Fig.2). Heat is applied on all surfaces between the weld metal and the base metal according to welding sequence.

Mechanical boundary conditions

(a) The specified mechanical boundary conditions are those just sufficient to prevent rigid body motion and rotations of the model: The nodes belonging to the element localized in the center of one lateral edge at the bottom horizontal plate are selected to prevent rigid body motion and rigid body rotations (see Fig. 6).

$$u = v = w = 0$$

$$\varepsilon_x = \frac{\partial u}{\partial x} = 0,\ \varepsilon_y = \frac{\partial v}{\partial y} = 0\ ,\ \varepsilon_z = \frac{\partial w}{\partial z} = 0$$

$$\omega_x = \frac{1}{2}\left(\frac{\partial w}{\partial y} - \frac{\partial v}{\partial z}\right) = 0,\ \omega_y = \frac{1}{2}\left(\frac{\partial u}{\partial z} - \frac{\partial w}{\partial x}\right) = 0, \text{ and}$$

$$\omega_z = \frac{1}{2}\left(\frac{\partial v}{\partial x} - \frac{\partial u}{\partial y}\right) = 0 \quad (11)$$

(b) Surfaces in contact with the surrounding (see Fig.6): The normal stresses to the surfaces in contact with the surrounding and the shear stresses are zero (i.e., in the plane y-z in x=0, $\sigma_x = \tau_{xy} = \tau_{xz} = 0$).

Solution of the finite element model of the 3-D unitary cell

After completing the finite element mesh and specifying the loading conditions (initial and boundary conditions and body loads), the solution can be initiated. In the transient thermal analysis, the time to complete each weld bead is 10 and 30 seconds for the structure with 24 and 8 weld beads, respectively. Thermal elastic plastic analysis for each simulation requires 55 load steps to complete the weld thermal cycles.

3.8. Localization of the points of interest in the 3-D unitary cell

The selected points of interest belong to important areas in the 3-D unitary cell (Fig. 7). Points 1 and 3 are located in the center of the horizontal plates, while points 2 and 4 are located in the center of the vertical plates. Points 5 and 8 and points 6 and 7 are located in the central part of the lower and upper flanges, respectively. Points 9, 12, 15 and 18, and points 11, 14, 17 and 20 are respectively located in the edges of the lower and upper flanges. Points 10, 13, 16 and 19 are located in the central part of the lateral edges of the vertical plates, while points 21, 22, 23 and 24 are located in the central part of the lateral edges of the horizontal plates. The magnitude of the distortion is positive when the displacement direction is inwards to the structure.

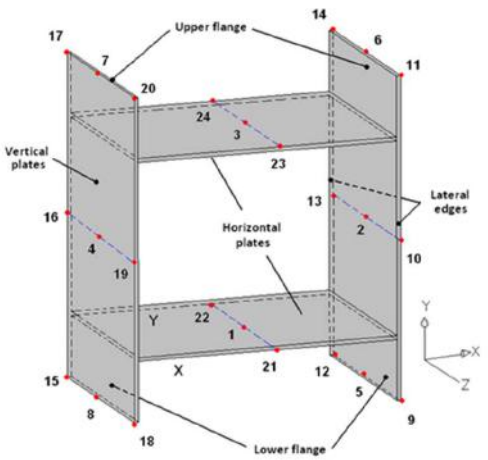

Figure 7. Localization of the points of interest in the 3-D unitary cell.

3.9. Configuration of the numerical simulation for the 3-D unitary cell

To demonstrate the hypothesis proposed in Section previous, four numerical simulations will be performed. Two of them deal with the proper welding sequence to reduce the distortion with 8 and 24 weld beads, and the other two deals with the proper welding sequence to reduce the residual stress with 8 and 24 weld beads. The numerical simulations for reduced distortion include the effects of the welding tacks. Table 1 depicts the configuration of the numerical simulations for the 3-D unitary cell.

Table 1- Configuration of the numerical simulations for the 3-D unitary cell

Numerical simulation	Proper welding sequence to reduce:	Number of welds	Welding tacks	Fig.
1	Distortion	8	Yes	11 (a)
2	Residual stress	8	No	11 (b)
3	Distortion	24	Yes	11 (c)
4	Residual stress	24	No	11 (d)

3.10. Numerical results of the different welding sequences analyzed in the 3-D unitary cell

The numerical results of interest are the maximum Von Misses residual stresses in the base metal, the distortion modes, and the maximum distortion in the unitary 3-D unitary cell.

Maximum Von Misses residual stress in the 3-D unitary cell

The maximum Von Misses residual stress in the base metal occurs in the central internal weld beads, at the boundary with the weld metal. Compressive residual stress occurs in the central region of the vertical and horizontal plates, while tensile residual stress occurs in the weld metal and nearby areas. Numerical simulation 2 (Fig. 8) results in the lowest residual stress, therefore confirming the hypothesis proposed in Section previous.

Distortion modes in the 3-D unitary cell

All the numerical simulations produce the same distortion mode. However, the magnitude of the distortion varies. The lower and upper flanges rotate inward to the structure, while the center plates bend towards the inside of the structure. The central regions of the vertical and horizontal flanges also bend inward towards the structure. Numerical simulation 3 (Fig. 9) results in the lowest distortion. This simulation deals with the proper welding sequence to reduce distortion, therefore confirming the hypothesis proposed in section previous.

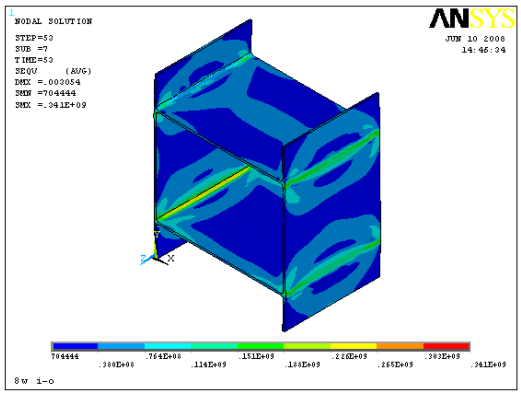

Figure 8. Distribution of residual stresses in numerical simulation 2.

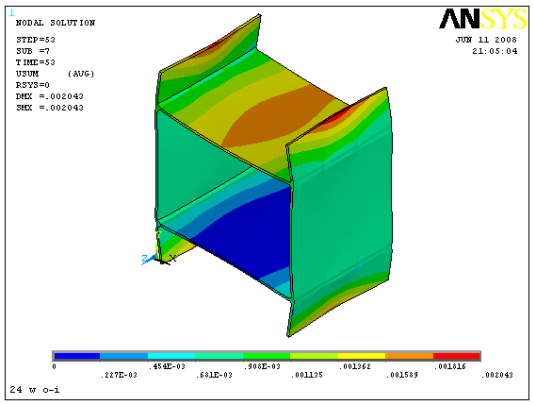

Figure 9. Isometric view of the distortion profile corresponding to numerical simulation 3.

Maximum distortion in the 3-D unitary cell

In all the simulations, the maximum distortion occurs in the central region of the upper and lower flanges (points 5, 6, 7 and 8). Simulation 3 produces the lowest distortion. However, this welding sequence results in the highest Von Misses residual stress. Once again, the proper welding sequence to reduce the residual stress results in highest distortion.

3.11. Numerical comparison between the proper welding sequence to reduce distortion and a special welding sequence in the 3-D unitary cell

The proper welding sequence to reduce distortion [Fig. 5(c)] recommends starting with the weld beads on sphere 4 (Fig. 4), located in the lateral edges of the outside of the structure. Next, the weld beads on sphere 3 are applied. These weld beads are located at the lateral edges, on the inside of the structure. Next, the weld beads located at the center box, on

the outside of the structure are applied (sphere 2). Finally, the weld beads on sphere 1, located in the center box, on the inside of the structure, are applied. The sequence involves applying alternating external and internal weld beads. For this reason, a special welding sequence (Fig. 10) that involves applying first the external and then internal weld beads is proposed. This welding sequence is commonly used to reduce the distortion in this type of joints. Weld beads belonging to the same sphere are applied in the same way in both welding sequences.

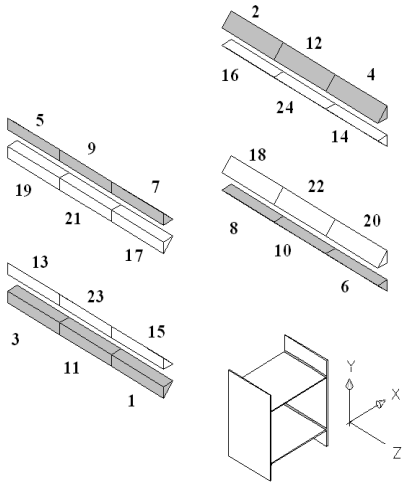

Figure 10. Configuration of a special welding sequence.

Table 2 shows the comparison of the numerical results between both welding sequences. It can be seen that the proper welding sequence results in the lowest distortion, verifying the original hypothesis.

Table 2. Comparison of numerical results between both welding sequences in the 3-D unitary cell.

Welding sequence	Maximum distortion (mm)	Difference (%)
Proper to reduce distortion	2.04	6.4
Special	2.18	

4. Experiments of the 3d unitary cell specimens

The 3-D unitary cell specimens have the same configuration analyzed in numerical simulations. The main objective of using the same configuration is performing a quantitative and qualitative comparison between numerical and experimental results.

4.1. Configuration of the experiment

Eight specimens and four welding sequences are studied: two of them are appropriate to reduce distortion, and the other two are appropriate to reduce residual stress (Table 3). These welding sequences are the same employed in the numerical simulations. Other parameters considered in these experiments are: the number of weld beads (8 or 24) and whether a relief of the residual stresses induced by manufacture, transportation, handling, storage and cutting is performed. Welding tacks are applied to all specimens before welding. The specimen number represents the order in which they are fabricated. Specimens T1, T2 and T3 were discarded due to measurement errors.

Table 3. 3-D unitary cell specimen configuration.

Specimen	Number of the Weld beads	Welding sequence most appropriate to reduce:	Residual stress relief	Welding tacks
T7	8	Distortion	No	Yes
T11	8	Distortion	Yes	Yes
T8	8	Residual stress	No	Yes
T4	8	Residual stress	Yes	Yes
T9	24	Distortion	No	Yes
T5	24	Distortion	Yes	Yes
T10	24	Residual stress	No	Yes
T6	24	Residual stress	Yes	Yes

Table 4 depicts the welding parameters employed.

Table 4. Welding parameters employed.

Material	S235 Steel (ST3S steel)
Welding process	GMAW-MAG
metal transfer mode	Short Circuiting Transfer
Arc voltage	22V
Welding current	160 A
Welding speed	5 mm/s
wire feed rate	50 mm / s
Contact tip to work distance (CTWD)	11 mm
Travel angle	Perpendicular
Work angle	45°
Electrode diameter	0,9 mm

4.2. Final distortion in the 3-D unitary cell specimens

The measurements were performed periodically (24, 48, 96 and 384 hours) after welding to observe possible rheological

effects. However, the distortion did not show any variation with time. Therefore, the rheological effects are discarded in the experimental tests.

The final distortion is calculated with equation (12):

$$\textit{Final distortion} = \textit{Distortion after applying the welding tacks} \pm \textit{Distortion after applying welding} \quad (12)$$

Fig. 11 depicts the comparison of the non-distorted and final distortion of specimen T9, showing a general agreement with distortions mode.

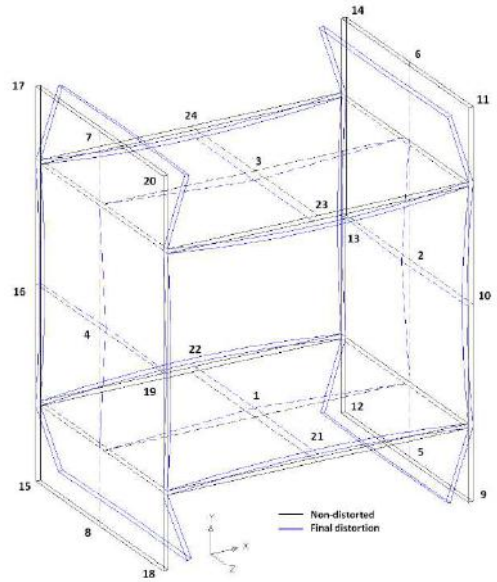

Figure 11. Final distortion (exaggerated) for welded specimen T9.

4.3. Comparison of distortion

Numerical distortion at the 24 points of interest can be directly compared with the experimental results. It is important to mention that the numerical simulations do not consider relief of the initial residual stresses. For this reason, only four numerical simulations were developed vs eight experiments. Therefore, each of the simulations will be compared against two experiments: with or without stress relief. Equation (13) is used to determine the percentage difference between numerical and experimental results for each of the 24 points of interest:

$$\textbf{Difference}(\%) = \frac{\textbf{Experimental result} - \textbf{Numerical result}}{\textbf{Experimental result}} \textbf{X100} \quad (13)$$

Table 5 depicts the difference percentage between numerical and experimental results. Of the 192 points of interest, 17 points show a good correlation in distortion between numerical and experimental results, 87 points present a difference between 0,1-10%, 61 points differ by 10,1-20%, 17 points are different by 20,1-30%, 2 points present a difference between 30,1-40%, and 4 points cannot be compared. The resulting comparison is considered acceptable. Welded specimens without stress-relief present smaller differences than specimens fabricated with stress-relief, with the exception of specimen T10 and the maximum differences in distortion occur in the points located at the center of the horizontal and vertical plates because the magnitude of the distortion in these points is very small. As an example, variations as small as 0,01 mm result in large percentage differences.

Fig. 12 shows a comparison between numerical (simulation 3) and experimental distortion (specimen T9). The figure shows good correlation between both results.

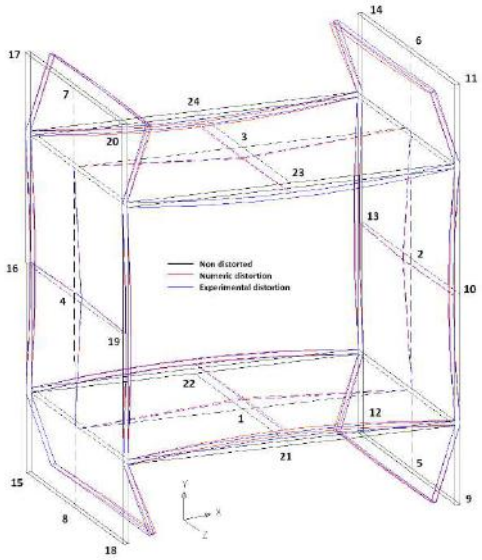

Figure 12. Comparison between numerical (simulation 3) and experimental distortion (specimen T9). Exaggerated distortion.

4.4. Procedures to determine the proper welding sequences to reduce residual stress, distortion, or a relation between both parameters in 2 and 3 dimensional symmetrical structures

Based on the welding sequence analysis developed in the stiffened symmetrical flat frame and 3-D unitary cell, the following procedures are obtained to determine proper welding sequences in 2 and 3 dimensional symmetrical structures. To determine the proper welding sequence to reduce the residual stress, distortion, or a relation between both parameters in symmetrical structures in 2 and 3 dimensions, all procedures are as follow: determine the axis of symmetry and the center of gravity of the structure. Draw concentric circles/spheres centered on the center of gravity of the structure and extending to the center of gravity of each of the weld beads. The weld beads located at the same distance from the center of gravity of the structure fall on the same circle/sphere. The circles/spheres are numbered from the smallest to the largest.

To reduce residual stress: Start with the weld bead on the smallest circle/sphere and then continue with the weld beads on the larger adjacent circle/sphere until the largest circle/sphere is reached. The weld beads on the same circle/sphere should be symmetrical. First, the weld beads with diagonal symmetry are selected. If the weld bead with diagonal symmetry has already been selected, then the farthest symmetrical weld bead is selected next. When a current weld bead has more than one farthest symmetrical weld bead, the adjacent weld bead in counter-clockwise direction is selected. Finally, to move from one circle/sphere to the other, the farthest weld bead to the current weld bead is selected. If a current weld bead has more than one farthest weld bead, the adjacent weld bead in counter-clockwise direction is selected. The converse welding method between weld beads is adopted.

To reduce Distortion: Apply welding tacks to the structure before welding. First, the weld beads in the largest circle/sphere are selected, followed by the weld beads on the adjacent smaller circle/sphere, until the smallest circle/sphere is reached. The application of the weld beads on the same circle/sphere should be in symmetrical form. The weld beads with diagonal symmetry are selected first. If the weld bead with diagonal symmetry has already been selected, then the farthest symmetrical weld bead is selected next. When a current weld bead has more than one farthest symmetrical weld bead, the adjacent weld bead in counter-clockwise direction is selected next. Finally, to move from one circle/sphere to the other, the farthest weld bead to the current is selected. If a current weld bead has more than one farthest weld bead, the adjacent weld bead in a clockwise direction is selected. The converse welding method between weld beads is adopted.

To improve the Residual Stress-Distortion relation: First, the weld beads on the smallest circle/sphere are selected and then continuing with the weld beads on the larger adjacent circle/sphere until the largest circle/sphere is reached. The application of weld beads on the same circle/sphere should be in an adjacent form in counter-clockwise direction. To move from one circle/sphere to the other, the closest weld bead to the current is selected. The converse welding method between weld beads is adopted.

5. Conclusions

Based on the results presented here in, we can conclude the following:

- Numerical simulations using 24 weld beads reduce distortion by up to 31% and residual stress by up to 18% with respect to numerical simulations using 8 weld beads.
- Numerical simulations of the proper welding sequence to reduce residual stress for 3-D structures confirm the hypothesis in Section 7.1 by delivering minimum stress and the proper welding sequence to reduce distortion also confirm the hypothesis proposed in Section 7.1 by producing minimum distortion.
- Structures with a greater number of sub-welds are more appropriate to reduce distortion, but also reduce the fatigue performance due to presence of the higher residual stresses which may reach the yield point in normal operating conditions. Therefore, to avoid the loss of stability, laying 8 weld beads seems to be more appropriate than the joint with 24 sub-welds.

REFERENCES

[1] Zhili, F., 2005, "Processes and Mechanisms of Welding Residual Stress and Distortion", CRC Press
[2] Masubuchi, K., 1980, "Analysis of Welded Structures: Residual Stresses, Distortion, and their Consequences", Pergamon Press.
[3] Masubuchi, K., 2001, "Welding Handbook: Residual Stress and Distortion", American Welding Society, 9th edition.
[4] Messler, R., 1999, "Principles of Welding: Processes, Physics, Chemistry, and Metallurgy", John Wiley and Sons, Inc.
[5] Tso, L. T., Peng, H. C., Wen, C. T., 2003, "Effect of welding sequence on residual stresses", Computer and Structures, 81: 273-286.
[6] Ji, S. D., Fang, H. Y., Liu, X. S., Meng, Q. G., 2005, "Influence of a welding sequence on the welding residual stress of a thick plate", Modeling and Simulation in Materials Science and Engineering, 13: 553-565.
[7] Nami, M. R., Kadivar, M. H., Jafarpur, K., 2004, "3D thermo-viscoplastic modeling of welds: Effect of piece-wise welding on thermo-mechanical response of thick plate weldments", Iranian Journal of Science and Technology, Transaction B, Vol. 28, No. B4, 467-478
[8] Mochizuki, M., Hayashi, M., 2000, "Residual stress distribution depending on welding sequence in multi-pass welded joints with X-shaped groove", ASME J. Pressure Vessel Technology. 122: 27-32.
[9] Mochizuki, M., Hattori, T., Nakakado, K., 2000, "Residual stress reduction and fatigue strength improvement by controlling welding pass sequence", ASME J. Engineering Materials and Technology, 122: 108-112.
[10] Tsai, C. L., Park, S. C., Cheng, W. T., 1999, "Welding distortion of a thin-plate panel structure", Weld. J. 78 (11): 156s-165s.
[11] Hackmair, C., Werner, E., Pönisch, M., 2003, "Application of welding simulation for chassis components within the development of manufacturing methods", Computational materials Science, 28: 540-547.
[12] Bart, O. N., Deepak, G., Kyoung, Y. K., 2004, "Welding distortion minimization for an aluminum alloy extruded beam structure using a 2D model", ASME J. Manufacturing Science and Engineering, 126: 52-63.
[13] Kadivar, M. H., Jafarpur, K., Baradaran, G. H., 2000, "Optimizing welding sequence with genetic algorithm", Computational Mechanics. 26: 514-519.
[14] Voutchkov, I., Keane, A. J., Bhaskar, A., Olsen, T. M., 2005, "Weld sequence optimization: the use of surrogate models for solving sequential combinatorial problems",

Computer methods in applied mechanics and engineering, 194: 3535-3551
[15] Murugan, V., Gunaraj, V., 2005, "Effects of Process parameters on angular distortion of gas metal arc welded structural steel plates", Weld. J. 84 (11): 165s-171s.
[16] Tso-Liang Teng., Ching-Cheng Lin., 1998, "Effect of welding condition on residual stress due to butt welds", Int. J. Pressure Vessels and Piping, 75: 857-864.
[17] Siddique M., Abid M., Junejo H. F., Mufti A., 2005, "3-D Finite element simulation of welding residual stresses in pipe-flange joints: effects of welding parameters", Materials Science Forum, Vols. 490-491, pp 79-84.
[18] Bhide, S. R., Michaleris, P., Posada, M., Deloach, J., 2006, "Comparison of buckling distortion propensity for SAW, GMAW, y FSW", Weld. J. 85 (9): 189s-195s.
[19] Jang, B., Kim, H. K., Kang S., 2001, "Effects of root opening on mechanical properties, deformation and residual stress of weldments", Weld. J. 80 (7): 80s-88s.
[20] Wahab, M. A., Alam, M. S., Painter, M. J., Stafford, P. E., 2006, "Experimental and numerical simulation of restraining forces in gas metal arc welded joints", Weld. J. 85 (2): 35s-43s.
[21] Muhammad, Abid., Muhammad, Siddique., 2005, "Numerical simulation of the effect of constraints on welding deformations and residual stresses in a pipe-flange joint", Modeling Simul. Mater. Sci. Eng. 13: 919-933.
[22] Cheng C.M., 2007, "Butt-welding residual stress of heat treatable aluminum alloys" J. Mater. Sci. Technol., Vol.23, No.2: 217-222.
[23] Michaleris, P., Sun, X., 1997, "Finite Element Analysis of Thermal Tensioning Techniques Mitigating Weld Buckling Distortion", Weld. J. 76(11): 451s-457s.
[24] Michaleris, P., Dantzig, J., Tortorelli, D., 1999, "Minimization of welding residual stress and distortion in large structures", Weld. J. 78 (11): 361-366.
[25] Shaoqing G., Xiaohong L., 2000, "Welding Distortion Control of thin Al alloy plate by static thermal tensioning", J. Mater. Sci. Technol, Vol.17, No. 1: 163-164.
[26] Engelhard G., Habip L. M., Pellkofer D., Schmidt J., Weber J., 2000, "Optimization of residual welding stresses in austenitic steel piping: prooftesting and numerical simulation of welding and postwelding processes", Nuclear Engineering and Design, Vol. 198: 141-151.
[27] Lin Y. C., Lee K. H., 1997,"Effect of preheating on the residual stress in type 304 stainless steel weldments", Journal of Materials Processing Technology, Vol. 63: 797-801.
[28] Adedayo S. M., Adeyemi M. B., 2000, "Effects of Preheat on residual stress distributions in arc-welded mild steel plates", ASM International. Journal of Materials Engineering and Performance, Vol. 9 (1): 7-11.
[29] Cho J. R., Lee B. Y., Moon Y. H., Van Tyne C. J., 2004, "Investigation of residual stress and post weld heat treatment of multi-pass welds by finite element method and experiments", Journal of Materials Processing Technology, 155-156: 1690-1695.
[30] Cheng X., Fisher J. W., Prask H. J., Gnäupel-Herold T., Yen B. T., Roy S., 2003, "Residual stress modification by post-weld treatment and its beneficial effect on fatigue strength of welded structures", International Journal of Fatigue, Vol. 25:1259-1269.
[31]Olabi, A. G., Hashmi M. S. J., 1998, "Effects of the stress-relief conditions on a martensite stainless-steel welded component", Journal of Materials Processing Technology, Vol. 77: 216-225.
[32] Aoki, S., Nishimura T., Hiroi T., Hirai S., 2007, "Reduction method for residual stress of welded joint using harmonic vibrational load", Nuclear Engineering and Design, Vol. 237: 206-212
[33] Xuesong L., Hongyuan F., Shude J., and Zhibo D., 2003, "Control of titanium alloy thin plate welding distortion by trailing penning", J. Mater. Sci. Technol., Vol.19, Suppl. 1: 184-186.
[34] Quanhong L., Jing C., Huanining C., 2001,"Possibility of inducing compressive residual stress in welded joints of SS400 steels", J. Mater. Sci. Technol., Vol.17, No.6: 661-663.
[35] Zhang J., Liu K., Zhao K., Li X., Liu Y., Zhang K., 2005, "A study on the relief of residual stresses in weldments with explosive treatment", International Journal of Solids and Structures, Vol. 42:3794-3806.
[36] Karlsson, L., 1986, "Thermal Stresses I-Chapter 5: Thermal Stresses in welding", Edited by Hetnarski R. B., Elsevier Science Publishers B.V.
[37] Argyris, J. H., Szimmat, J., William, K. J., 1982, "Computational aspect of welding stress analysis", Computer methods in applied mechanics and engineering, 33: 635-666.
[38] Boley, B., Weiner, J., 1962, "Theory of thermal stresses", John Wiley and Sons, Second Edition.
[39] Swanson Analysis Systems, Inc. "III ANSYS user´s manual: Elements", Vol.
[40] Chang, P. H., 2003, "Numerical and experimental investigation on residual stresses of the butt-welded joints", Computation Material Science, 29: 511-522
[41] Hernández, A. I., 2009, "Welding Sequence Analysis", Doctoral thesis, AGH-University of Science and Technology, Poland.

Table 5. Difference (%) between numerical and experimental results

Point	Specimen							
	T7	**T11**	**T8**	**T4**	**T9**	**T5**	**T10**	**T6**
1	20	20	0	0	-20	-20	20	20
2	26,6	26,6	---	---	-5	-5	0	0
3	20	20	-40	-40	-20	-20	20	20
4	-10	26,6	---	----	-5	-5	0	0
5	-5,7	2,6	1,6	3,1	-8,4	-8,4	13,1	1,8
6	-3,6	-6.4	-8,1	-8,1	-10,7	-2,9	-12,2	-1,1
7	-1,1	11,2	0	5,2	-2,4	-9,1	0,6	6,3
8	-7.5	-0,5	-8.2	-2.6	-4,8	-13	-12,5	2,7
9	2,8	6,2	0	5,5	-1,3	1,9	2,6	6,6
10	-3,3	11,4	-20	10	12,5	-16,6	-26,6	-26,6
11	-2,6	-2,6	-12,9	-6,6	-5,5	-2	-2,7	19,3
12	-14,6	9,7	2,1	-0,5	-10,7	-13,3	23,4	11,2
13	20	20	30	30	20	20	-26,6	-26,6
14	14	-8,2	-8,3	-8,3	-16	-8,7	-12,7	0,8
15	-16,2	8,5	-7.4	1	0	-20	1,8	10
16	-11,4	2,5	0	0	-20	25	20	20
17	8,2	21,7	0	8,3	-2,6	-6,2	-7,6	13
18	-4	-4	-14,1	-4,8	-8,7	-8,7	-21	6,9
19	5	24	0	33	20	20	20	20
20	-8,8	8,1	-1,6	1,1	-7,6	-11,4	12,1	15,8
21	-14	-26.6	0	0	-32	5,7	-16	3,3
22	-7,2	-18	-13,3	-13,3	-7,2	1,6	-13,3	-13,3
23	-14	-26.6	-24	-3,3	0	0	-10	-10
24	-4	-15,5	-10	26,6	-23.6	-13,3	17,1	3,3

